Spectroscopy and orange-blue frequency upconversion in Pr^{3+}-doped GeO_2-PbO-Nb_2O_5 glass

Spectroscopy and orange–blue frequency upconversion in Pr^{3+}-doped GeO_2–PbO–Nb_2O_5 glass

R Balda†‡, I Sáez de Ocáriz†, J Fernández†‡, J M Fdez-Navarro§ and M A Arriandiaga‖

† Departamento de Física Aplicada I, ETSII y Telecomunicación, Universidad del País Vasco, Alameda Urquijo s/n, 48013, Bilbao, Spain
‡ Centro Mixto CSIC-UPV/EHU, ETSII y Telecomunicación, Universidad del País Vasco, Alameda Urquijo s/n, 48013, Bilbao, Spain
§ Fundación Centro Nacional del Vidrio, La Granja, Segovia, Spain
‖ Departamento de Física Aplicada II, Facultad de Ciencias, Universidad del País Vasco, Apartado 644, Bilbao, Spain

Abstract. The visible luminescence of Pr^{3+}-doped lead–germanate glass of composition (in mol%) $60GeO_2$–$25PbO$–$15Nb_2O_5$ has been investigated for different Pr^{3+} concentrations and temperatures by using steady-state and time-resolved laser spectroscopy. The fluorescence from the $^1D_2$ level shows a strong concentration quenching for Pr^{3+} concentrations higher than 0.1 mol%. The time evolution of the decays from the $^1D_2$ level and the concentration dependence of the effective decay rates are consistent with a dipole–dipole quenching process in the framework of a diffusion-limited regime. Anti-Stokes emission from the $^3P_0$ level following excitation of the $^1D_2$ state has been observed for the samples doped with 0.1, 0.5, 1, and 2 mol% of Pr^{3+}. The temporal behaviour of the upconverted emission from the $^3P_0$ level together with its quadratic dependence on the excitation energy and its linear dependence on Pr^{3+} concentration suggest that an excited-state absorption (ESA) is the dominant mechanism for the upconversion process in this glass.

1. Introduction

The development of high-capacity telecommunication networks has generated a large amount of research devoted to finding new rare-earth-doped glasses for use in optical fibre amplifiers. Glasses with phonon energies lower than that of silica offer the possibility of developing more efficient lasers and fibre optic amplifiers at wavelengths not accessible with silica. Among the oxide glasses, the rare-earth-doped lead–germanate glasses have been the subject of several recent investigations [1–11]. These glasses have smaller maximum vibrational frequencies than those shown by silicate, phosphate, and borate glasses [12, 13]. The reduced phonon energy increases the quantum efficiency of the luminescence from excited states of rare-earth (RE) ions and the upconversion efficiency, which is low in conventional oxide glasses. Lead–germanate glasses combine high mechanical strength, high chemical durability, and temperature stability with good transmission in the infrared region [14] up to 4.5 μm, which make them promising materials for technological applications such as in new lasing materials, upconverting phosphors, and optical waveguides [1–4].

Trivalent praseodymium is an attractive optical activator which offers the possibility of simultaneous blue, green, and red emission for laser action, as well as infrared emission for optical amplification at 1.3 μm [15]. Pr^{3+} systems are also interesting as short-wavelength

upconversion laser materials [16–18]. One of the general features of some fluorescing levels of the Pr^{3+} ion is that the emission is quenched when concentration and/or temperature increase. Among the energy-transfer mechanisms responsible for this quenching, cross-relaxation and upconversion are very important. Upconversion is particularly interesting since it may lead to the observation of anti-Stokes fluorescence, which has many applications in upconversion lasers [19, 20]. In addition, it is a very useful tool in studying the higher-energy states of the optically active centres in solids [21].

The upconverted emissions are in general attained by different mechanisms:

  (i) sequential absorption of pump photons in one ion involving excited-state absorption (ESA),
 (ii) photon avalanche, and
(iii) energy-transfer upconversion (ETU).

In the case of the upconverted blue emission from the $^3P_0$ level, after orange excitation at the level $^1D_2$, energy transfer as well as stepwise absorption of photons may be operative [22–26]. Upconverted blue emission following orange–yellow excitation is explained for borate [23], fluoroindate [24], fluorophosphate [25], and lead–germanate [9] glasses in terms of energy transfer, whereas in the case of tellurite glasses [26] a sequential two-photon excitation process is proposed as the dominant mechanism of the upconversion.

In this work, together with the optical properties of the visible luminescence from Pr^{3+}-doped lead–germanate-based glass of composition $60GeO_2$–$25PbO$–$15Nb_2O_5$, we report a dynamical study of the energy-transfer mechanism for different Pr^{3+} concentrations. This study includes absorption, emission, lifetime results, and fluorescence quenching of the $^1D_2$ emission. We also present the results of orange-to-blue upconversion obtained by pumping the $^1D_2$ state. The time evolution of the upconverted fluorescence indicates that a sequential two-photon excitation process is the dominant mechanism of the upconversion in this glass.

2. Experimental techniques

Batches of 20 g of glass have been prepared by mixing the high-purity reagents GeO_2 (ALFA 99.999), PbO (ALFA 99.9995), and Nb_2O_5 (ALFA 99.999); the glass was doped with 0.05, 0.1, 0.5, 1, and 2% Pr_2O_3 (ALFA 99.999). This mixture was melted in a platinum crucible placed in a vertical tubular furnace at temperature between 1100 and 1300 °C for 1 h and then poured onto a preheated brass plate; this was followed by 1 h of annealing at 450 °C and a further cooling at 1.5 °C min^{-1} down to room temperature. Finally the samples were cut and polished for optical measurements.

The sample temperature was varied between 4.2 K and 300 K with a continuous-flow cryostat. Conventional absorption spectra were taken with a Cary 5 spectrophotometer. The steady-state emission measurements were made with an argon laser as the exciting light. The fluorescence was analysed with a 0.25 m monochromator, and the signal was detected by a Hamamatsu R928 photomultiplier and finally amplified by a standard lock-in technique.

Lifetime measurements and orange-to-blue upconversion studies were performed by exciting the samples with a pulsed frequency-doubled Nd:YAG-pumped tunable dye laser of 9 ns pulse width and 0.08 cm^{-1} linewidth. The fluorescence was analysed with a 1 m Spex monochromator, and the signal was detected by a Hamamatsu R928 photomultiplier. The decay time measurements were performed by using the averaging facilities of a Tektronix 2400 digital storage oscilloscope. Upconverted emission spectra were detected by an EGG-PAR optical multichannel analyser.

3. Results

3.1. Absorption and emission properties

The room temperature absorption spectra were obtained for all concentrations in the 400–2500 nm range by making use of a Cary 5 spectrophotometer. As an example, figure 1 shows the absorption coefficient as a function of wavelength at room temperature for the sample doped with 2 mol% of Pr^{3+}. It consists of several bands corresponding to transitions between the $^3H_4$ ground state and the excited multiplets belonging to the $4f^2$ configuration of Pr^{3+} ions. The broad lines are due to large site-to-site variations of the crystal-field strengths. The positions of the bands and the corresponding bandwidths do not change with concentration, indicating that the dopants are homogeneously distributed. In order to estimate the content of praseodymium in the different samples, we have calculated the integrated absorption coefficient for different absorption bands and a linear dependence on concentration was found, which indicates that the relative concentrations of Pr^{3+} are in agreement with the nominal values.

The room temperature steady-state emission spectra were obtained in the 460–800 nm spectral range by exciting with an argon laser. Figure 2 shows, as an example, the emission spectra for the samples doped with 0.1, 0.5, and 2 mol% of Pr^{3+}. As can be seen, after excitation at the $^3P_2$ level (454 nm) there is emission from $^3P_0$ and $^1D_2$ levels. In addition, the spectra at room temperature present some weak peaks corresponding to transitions from the $^3P_1$ level. At low concentration the most intense emission corresponds to the $^1D_2 \rightarrow {}^3H_4$ transition, but as concentration rises this emission shows a strong quenching and at high concentration the most prominent one is the emission from the $^3P_0$ level. This concentration quenching of the $^1D_2$ emission is often observed in the emission spectra of Pr^{3+} and has been attributed to cross-relaxation between Pr^{3+} ions [27–30].
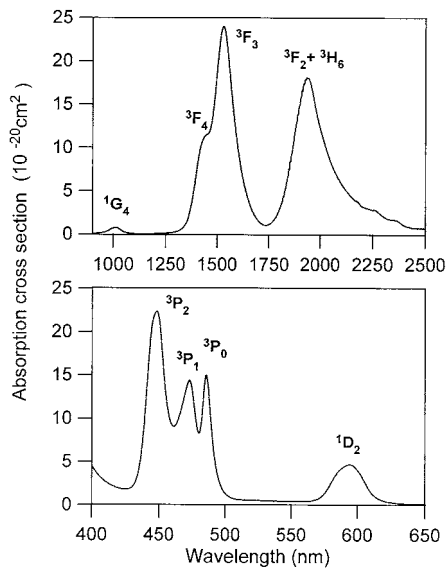

Figure 1. The room temperature absorption spectrum of the sample doped with 2 mol% of Pr^{3+}.
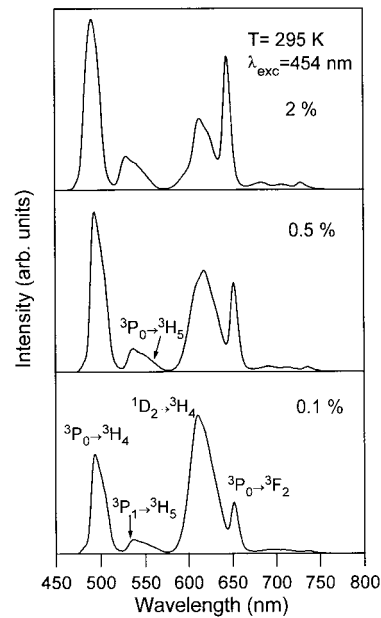
Figure 2. Steady-state emission spectra of the samples doped with 0.1, 0.5, and 2 mol% of Pr^{3+} obtained at room temperature by exciting the samples at 454 nm.

3.2. Lifetime results

In order to obtain additional information about the luminescence properties of Pr^{3+} ions in this glass, the fluorescence dynamics of the $^3P_0$ and $^1D_2$ emitting levels were investigated for different Pr^{3+} concentrations at different temperatures. Decay curves for all samples were obtained under laser pulsed excitation at 454 nm ($^3P_2$) and 598 nm ($^1D_2$), and luminescence was collected at different emission wavelengths between 490 and 720 nm. Figure 3 shows the lifetime values of the $^3P_0$ and $^1D_2$ levels as functions of concentration at 77 K. As can be observed, the lifetimes of the $^3P_0$ level are nearly independent of concentration up to 1 mol%; however, the decays of the $^1D_2$ level become shorter with increasing concentration even at low temperature, which indicates the presence of energy-transfer processes at concentrations higher than 0.1 mol%. At very low concentration and temperature, the decays of the $^1D_2$ level can be described by an exponential function within the experimental error. As concentration increases up to 1 mol% they become non-exponential and a rapid decrease of the lifetimes occurs. However, for the sample doped with 2 mol%, the decay approaches again a single-exponential function. Figure 4 shows a logarithmic plot of the experimental decays of the $^1D_2$ level for the samples doped with 0.5, 1, and 2 mol% at 77 K. The lifetime values correspond to the average lifetime defined by

$$\tau_{avg} = \left(\int t I(t)\, dt \right) \bigg/ \left(\int I(t)\, dt \right).$$

The lifetimes of the two levels are almost independent of temperature between 77 and 300 K.

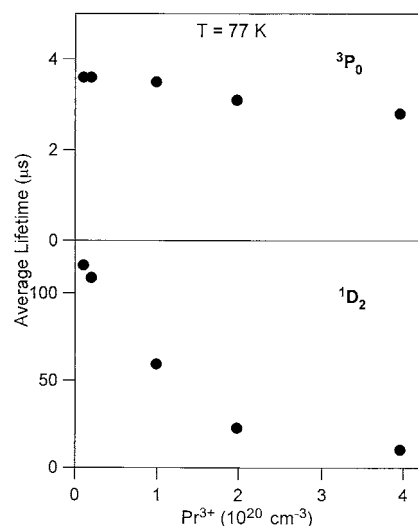**Figure 3.** Average lifetime values of the $^3P_0$ and $^1D_2$ levels as functions of concentration at 77 K. Lifetimes were obtained by exciting at 454 nm and 598 nm respectively.
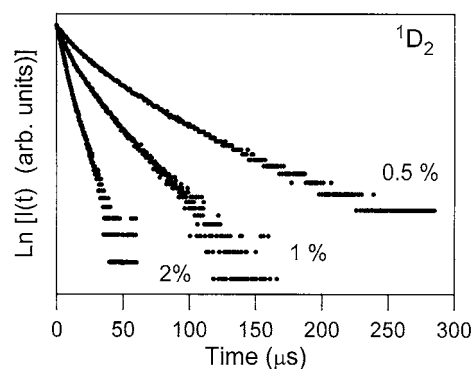
Figure 4. A logarithmic plot of the fluorescence decays of the $^1D_2$ level for samples doped with 0.5, 1, and 2 mol% of Pr^{3+}. The decays were obtained by exciting at the $^1D_2$ level (598 nm) at 77 K.

As in other Pr^{3+} systems investigated [27–30], the $^1D_2$ emission is affected much more strongly by quenching than is $^3P_0$, so we will focus the discussion on the $^1D_2$ level and its fluorescence dynamics.

3.3. Orange-to-blue frequency upconversion

To investigate the possibility of upconverted fluorescence in this system, we have excited the $^1D_2$ level and we have observed anti-Stokes fluorescence from the $^3P_0 \rightarrow {}^3H_4$ transition in the 77 K–295 K temperature range for the samples doped with 0.1, 0.5, 1, and 2 mol% of Pr^{3+}. Figure 5 shows the upconverted emission spectra for the samples doped with 0.5, 1, and 2 mol% at 77 K obtained by exciting at 598 nm. The upconverted emission has the same lineshape and peak position as that obtained by one-photon excitation of the level $^3P_0$.
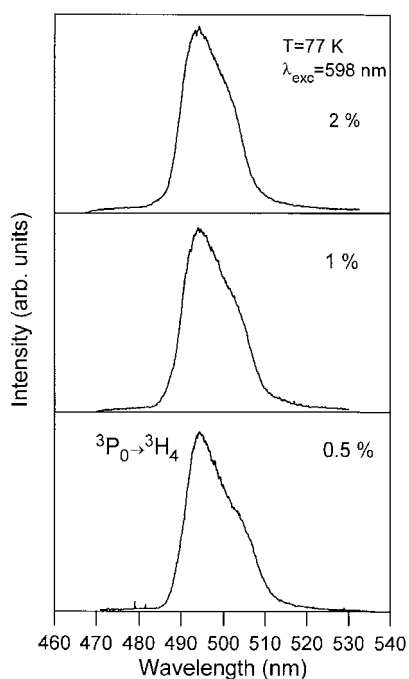

Figure 5. Fluorescence spectra corresponding to the $^3P_0 \rightarrow {}^3H_4$ transition for three different concentrations at 77 K. The excitation wavelength (598 nm) was in resonance with the transition $^3H_4 \rightarrow {}^1D_2$.

The intensity of the anti-Stokes emission shows a quadratic dependence on the excitation laser energy indicating that two photons participate in this process [22]. Figure 6 shows a logarithmic plot of the integrated emission intensity of the upconverted fluorescence as a function of the pump laser intensity. The intensity of the upconverted fluorescence has a linear dependence on the Pr^{3+} concentration in this concentration range.
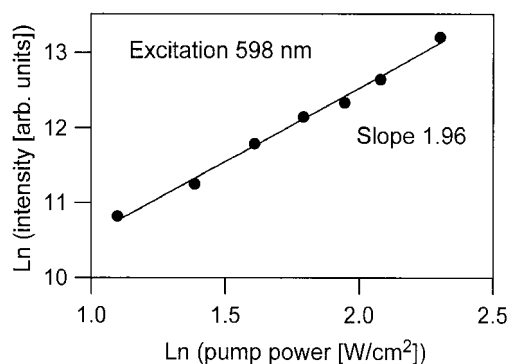

Figure 6. A logarithmic plot of the integrated intensity of the upconverted $^3P_0 \rightarrow {}^3H_4$ emission as a function of the pump laser intensity. Data correspond to 77 K and 1 mol% of Pr^{3+}.

The temporal evolution of the upconverted blue emission is illustrated in figure 7. As an example, the experimental decay of the $^3P_0$ level obtained at 77 K by exciting at 598 nm is shown for the samples doped with 0.5, 1, and 2 mol%. As can be observed the decay curves of the anti-Stokes $^3P_0 \rightarrow {}^3H_4$ emission do not show any rise time, and the lifetime is similar to that of the $^3P_0$ level under direct excitation. The same behaviour was observed at room temperature.
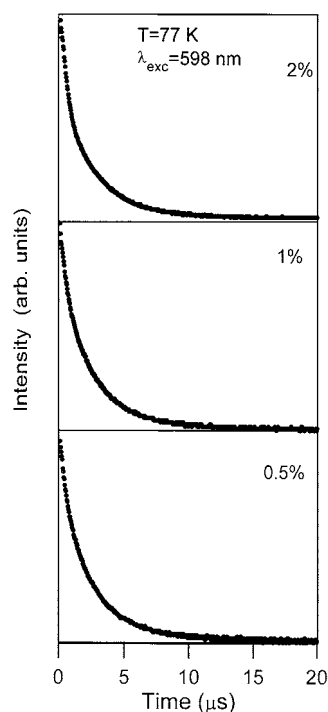

Figure 7. Experimental emission decay curves of the level $^3P_0$ obtained under excitation in resonance with the transition $^3H_4 \rightarrow {}^1D_2$ (598 nm) for the samples doped with 0.5, 1, and 2 mol% of Pr^{3+}. Data correspond to 77 K.

4. Discussion

4.1. Concentration quenching of the $^1D_2$ level

The characteristic decay time of the $^1D_2$ state of Pr^{3+} ions should be governed by a sum of probabilities for several competing processes: radiative decay, non-radiative decay by multiphonon emission, and non-radiative decay by energy transfer to other Pr^{3+} ions. The non-radiative decay by multiphonon emission from the $^1D_2$ level is expected to be small because of the large energy gap to the next $^1G_4$ lower level ($\approx$6950 cm^{-1}) as compared with the highest energies of the phonons involved ($\approx$890 cm^{-1}) [1, 5]. Hence, at low temperature and low concentration (0.05 mol%) the measured lifetime should approach the radiative lifetime of the $^1D_2$ level. As the concentration rises, the lifetime decreases even at low temperature which indicates that Pr–Pr relaxation processes play an important role. One or both of the following two mechanisms can be operative: (i) cross-relaxation between pairs of Pr^{3+} ions; (ii) migration of the excitation energy due to resonant energy transfer among Pr^{3+} ions until a quenching centre is reached (any other ion or defect to which the energy can migrate). Energy migration has been described either as a diffusion process or as a random walk (hopping model), and it was shown that these two models lead to similar results [31]. In the diffusion model, in

the case of dipole–dipole interaction, at long times after the pulse excitation the fluorescence of the donors decays exponentially with an asymptotic decay time, τ, given by [31]

$$\frac{1}{\tau} = \frac{1}{\tau_0} + VC_AC_D \tag{1}$$

where τ_0 is the intrinsic decay time, V is a constant involving donor–donor and donor–acceptor transfer constants, and C_A and C_D are the acceptor and donor concentrations respectively. The donor decay regime described by relation (1) is known as diffusion-limited decay [31]. In our case the donors and acceptors are the Pr^{3+} ions, and the equation gives the effective decay as a function of the square of concentration. Hence a logarithmic plot of the effective decay versus concentration should show a slope equal to two if the ^{1}D$_2$ decay is diffusion limited. An increase in the donor concentration produces a faster migration of energy and it was shown that in the case of very fast diffusion, the donor fluorescence decay is purely exponential and the effective decay shows a linear dependence on concentration [31].

As we have seen, in this glass for Pr^{3+} concentrations higher than 0.1 mol% and up to 1 mol%, the decays are non-exponential and therefore fast diffusion can be neglected in this concentration range. However, diffusion processes can be competitive with a direct transfer at concentrations higher than 1%.

Figure 8 shows a logarithmic plot of the effective fluorescence decay times as a function of the Pr^{3+} concentration. As can be observed, the slope is 1.71 which indicates that the Pr–Pr energy transfer occurs in the framework of a diffusion-limited regime.
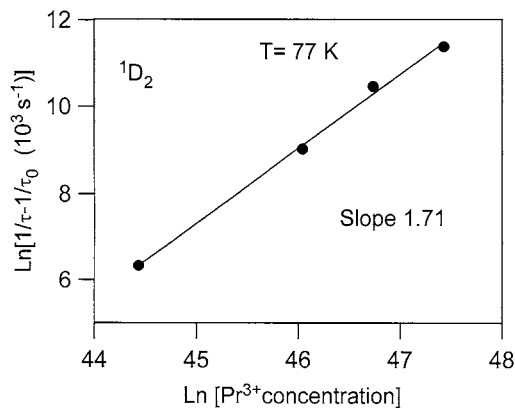

Figure 8. A logarithmic plot of the diffusion-limited probability of the ^{1}D$_2$ emission as a function of concentration at 77 K.

The change from exponential to non-exponential decays when the Pr^{3+} concentration increases up to 1 mol% can be mainly due to energy diffusion and cross-relaxation processes. In order to identify the mechanism of energy transfer between Pr^{3+} ions we have analysed the experimental decays of the ^{1}D$_2$ level for the samples doped with 0.5 and 1 mol% where a diffusion-limited process may occur. When diffusion is as fast as energy transfer, under the assumption of electrostatic multipole interaction the donor decay curves can be described by the expression [32]

$$I(t) = I(0) \exp\left[-\frac{t}{\tau_0} - \Gamma\left(1 - \frac{3}{s}\right)\frac{4}{3}\pi R_0^3 N \left(\frac{t}{\tau_0}\right)^{3/s} - Wt \right] \tag{2}$$

with $s = 6$, 8, and 10, respectively, for electric dipole–dipole, dipole–quadrupole, and quadrupole–quadrupole interactions. N is the acceptor concentration, R_0 is the critical transfer

distance for which the probability for energy transfer between a donor and acceptor is equal to the intrinsic decay probability $1/\tau_0$, and W is the probability of migration-limited relaxation which corresponds to VC_AC_D in equation (1). The intrinsic decay time is obtained from the low-temperature decay of the less concentrated sample (0.05 mol%).

The decay curves for the samples doped with 0.5 and 1 mol% were fitted to equation (2) with the critical radius R_0 and the rate of migration-limited energy transfer W as variable parameters for $s = 6$, 8, and 10. Figure 9 shows a least-squares fit of the experimental decays at 77 K for both samples. In all cases the best fit was for $s = 6$ for all temperatures. Similar values for the critical transfer radius are obtained ($R_0 = 11$ and 10.3 Å for the samples doped with 0.5% and 1% respectively), which support the dipole–dipole transfer hypothesis. The migration transfer rate is low for the sample doped with 0.5% ($W = 5.8 \times 10^3$ s^{-1}) and increases with concentration ($W = 24 \times 10^3$ s^{-1} for the sample doped with 1%). With account taken of the inherent errors in the preceding fit, these values are in agreement with the VC_AC_D probabilities given by the diffusion-limited model obtained from equation (1), which are 8×10^3 s^{-1} for the sample doped with 0.5% and 28×10^3 s^{-1} for the sample doped with 1%.

4.2. Upconversion mechanism

The upconverted emission from the $^3P_0$ level after excitation at $^1D_2$ can occur non-radiatively by an energy-transfer upconversion (ETU) as well as radiatively by an excited-state absorption (ESA) [21, 33]. In the first mechanism two ions are involved whereas a single ion is involved in the second one. As two laser photons are involved in each of the above processes, the $^3P_0$ fluorescence shows a quadratic dependence on pump laser energy as has been observed in various systems [22–26]. Lifetime measurements provide a useful tool for discerning which is the operative mechanism. Upconversion by energy transfer leads to a decay curve for the anti-Stokes emission which shows a rise time after the laser pulse, followed by a decay and a longer lifetime than that of the $^3P_0$ level under direct excitation [22]. The radiative ESA process occurs within the excitation pulse width, leading to an immediate decay of the upconverted luminescence after excitation.

Upconversion by energy transfer has been observed in borate [23], fluoroindate [24], and fluorophosphate [25] glasses and has been attributed to a redistribution of energy between two ions according to $^1D_2 + {}^1D_2 \rightarrow {}^3P_0 + {}^1G_4 +$ phonons. This process proposed to explain the ETU [34] considers the transfer inside pairs of ions after selective excitation by a pulsed laser. In this model, when both ions of a pair are excited to the $^1D_2$ state, a transfer occurs by which one ion loses energy and goes to the lower excited level $^1G_4$, while the other one gains energy and goes to the $^3P_2$ level from where, by non-radiative decay, the $^3P_0$ level is populated.

From the data presented in section 3.3, it is clear that in our system none of our results points to an upconversion dominated by an energy-transfer mechanism. As we have shown in figure 7, the temporal evolution of the upconverted blue emission does not show any rise time and the lifetime is similar to the one obtained under direct excitation. In addition, the intensity of the upconverted fluorescence shows a linear dependence on the Pr^{3+} concentration, whereas in the case of energy-transfer upconversion, the upconverted fluorescence should have a quadratic dependence on concentration. These results suggest that an excited-state absorption (ESA) mechanism is responsible for the upconversion process. An analysis of the energy level diagram for this glass shows that the most likely ESA mechanism to populate the $^3P_0$ level after excitation with orange photons should involve the $^3H_6$ state. In this process, one Pr^{3+} ion, initially in the ground state, absorbs one orange photon and is excited to the $^1D_2$ level from where the $^3H_6$ level is populated by fast non-radiative relaxation. This is followed by

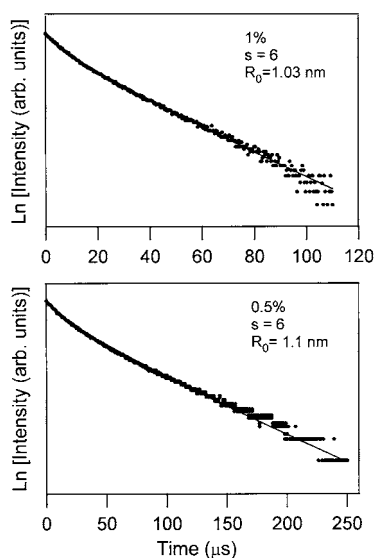**Figure 9.** A logarithmic plot of the experimental emission decay curves of the level $^1D_2$ and the calculated fit for dipole–dipole interaction ($s = 6$) (solid line) in the samples doped with 0.5 and 1 mol% of Pr³⁺ at 77 K.
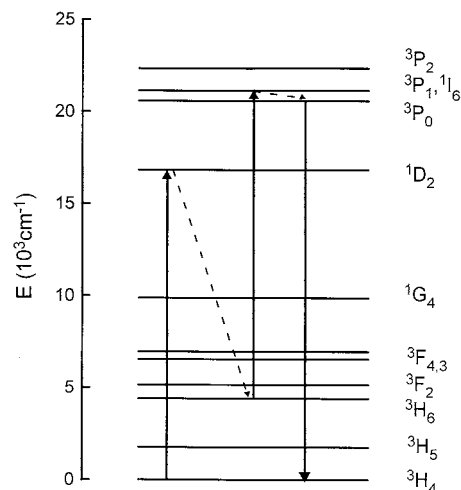
Figure 10. The energy level diagram and upconversion process (ESA) of Pr³⁺ in a GeO₂–PbO–Nb₂O₅ glass.

absorption of a second orange photon from the $^3H_6$ level to the $(^3P_1, ^1I_6)$ levels from where the $^3P_0$ level is populated non-radiatively. Figure 10 shows this mechanism in the energy level diagram constructed from the absorption and emission spectra of the 2% doped sample. This process has also been observed in a tellurite glass [26].

The temporal evolution of the decays in this glass, together with the quadratic dependence of the upconverted fluorescence on the excitation intensity and its linear dependence on the Pr³⁺ concentration, suggests that an ESA process is the dominant mechanism of the upconversion fluorescence at the concentrations and temperatures studied.

It is important to mention that the addition of cations such as niobium has been proven to increase both linear and non-linear refractive indices of glass materials by over 15%, depending upon the niobium concentration [35]. The higher linear refractive index gives rise to higher radiative emission rates for rare-earth energy levels. This could be related to an enhancement of the ESA upconversion mechanism compared to the ETU mechanism found in a binary lead–germanate glass [9]. To clarify the role of niobium in the dominant upconversion mechanism, further investigations with different niobium concentrations are needed.

5. Conclusions

From the above results, the following conclusions can be reached:

(i) Fluorescence quenching from the $^1D_2$ state has been demonstrated to occur for Pr³⁺ concentrations higher than 0.1 mol% even at 77 K. The time evolution of the decays from the $^1D_2$ state is consistent with a dipole–dipole energy-transfer mechanism in the framework of a diffusion-limited regime.

(ii) Anti-Stokes fluorescence from the $^3P_0 \rightarrow {}^3H_4$ transition under excitation of the $^1D_2$ level was observed. The temporal behaviour of the anti-Stokes emission, together with

the linear dependence on the Pr^{3+} concentration and the quadratic dependence of the upconverted fluorescence on the excitation laser intensity, indicates that an ESA is the dominant mechanism of the upconverted emission.

Acknowledgments

References

[1] Wang J, Lincoln J R, Brocklesby W S, Deol R S, Mackechnie C J, Pearson A, Tropper A C, Hanna D C and Payne D N 1993 *J. Appl. Phys.* **73** 8066
[2] McDougall J, Hollis D B and Payne M J P 1995 *Phys. Chem. Glasses* **36** 52
[3] Shepherd D P, Brick D J B, Wang J, Tropper A C, Hanna D C, Kakarantzas G and Townsend P D 1994 *Opt. Lett.* **19** 954
[4] Pan Z, Morgan S H, Loper A, King V, Long B H and Collins W E 1995 *J. Appl. Phys.* **77** 4688
[5] Pan Z, Morgan S H, Dyer K, Ueda A and Liu H 1996 *J. Appl. Phys.* **79** 8906
[6] Pan Z and Morgan S H 1997 *J. Lumin.* **75** 301
[7] Rolli R, Camagni P, Samoggia G, Speghini A, Wachtler M and Bettinelli M 1998 *Spectrochim. Acta* A **54** 2157
[8] Wachtler M, Speghini A, Gatterer K, Fritzer H P, Ajò D and Bettinelli M 1998 *J. Am. Ceram. Soc.* **81** 2045
[9] Balda R, Fernández J, de Pablos A and Fdez-Navarro J M 1999 *J. Phys.: Condens. Matter* **11** 7411
[10] Balda R, Fernández J, Sanz M, Oleaga A, de Pablos A and Fdez-Navarro J M 1999 *J. Non-Cryst. Solids* **256+257** 271
[11] Balda R, Fernández J, Sanz M, de Pablos A, Fdez-Navarro J M and Mugnier J 2000 *Phys. Rev.* B **61** 3384
[12] Ribeiro S J L, Dexpert-Ghys J, Piriou B and Mastelaro V R 1993 *J. Non-Cryst. Solids* **159** 213
[13] Canale J E, Condrate R A, Nassau K and Cornilsen B C 1986 *J. Can. Ceram. Soc.* **55** 50
[14] Lezal D, Pedlíková J and Horák J 1996 *J. Non-Cryst. Solids* **196** 178
[15] Kaminskii A A 1991 *Ann. Phys., Paris* **16** 639
[16] Allain J Y, Monerie M and Poignant H 1991 *Electron. Lett.* **27** 1156
[17] Smart R G, Hanna D C, Tropper A C, Davey S T, Carter S F and Szebesta D 1991 *Electron. Lett.* **27** 1307
[18] Remilleux A and Jacquier B 1996 *J. Lumin.* **68** 279
[19] Johnson L F and Guggenheim H J 1971 *Appl. Phys. Lett.* **19** 44
[20] Sandrock T, Scheife H, Heumann E and Huber G 1997 *Opt. Lett.* **22** 808
[21] Auzel F 1973 *Proc. IEEE* **61** 758
[22] Malta O L, Antic-Fidancev E, Lemaitre-Blaise M, Dexpert-Ghys J and Piriou B 1986 *Chem. Phys. Lett.* **129** 557
[23] Pacheco E M and de Araujo C B 1988 *Chem. Phys. Lett.* **148** 334
[24] de Araujo L E E, Gomes A S L and de Araujo C B 1994 *Phys. Rev.* B **50** 16 219
[25] Balda R, Fernández J, Adam J L, Mendioroz A and Arriandiaga M A 1999 *J. Non Cryst. Solids* **256+257** 299
[26] Kim S I and Yun S I 1994 *J. Lumin.* **60+61** 233
[27] Dornauf H and Heber J 1980 *J. Lumin.* **22** 1
[28] Hegarty J, Huber D L and Yen W M 1982 *Phys. Rev.* B **25** 5638
[29] de Mello Donegá C, Lambaerts H, Meijerink A and Blasse G 1993 *J. Phys. Chem. Solids* **54** 873
[30] Balda R, Fernández J, Sáez de Ocáriz I, Voda M, García A J and Khaidukov N 1999 *Phys. Rev.* B **59** 9972
[31] Weber M J 1971 *Phys. Rev.* B **4** 2932
[32] Dexter D L 1953 *J. Chem. Phys.* **21** 836
[33] Wright J C 1976 *Top. Appl. Phys.* **15** 239
[34] Buisson B and Vial J C 1981 *J. Physique Lett.* **42** L115
[35] Vogel E M, Kosiniski S G, Krol D M, Jackel J L, Friberg S R, Oliver M K and Powers J D 1989 *J. Non-Cryst. Solids* **107** 244